Advance Sustainable Science, Engineering and Technology (ASSET)
Vol. 7, No.4, October 2025, pp. 02504029-01 ~ 02504029-18
ISSN: 2715-4211 DOI: https://doi.org/10.26877/asset.v7i4.2399

Barium Removal from Produced Water Using RCC-Based Ceramic Adsorbent: Fixed-Bed Column Adsorption

Netty Herawati[1,3], Subriyer Nasir[1,2]*, Kiagus Ahmad Roni[3], Muhammad Arif Karim[3]

[1]Doctoral Engineering Program, Sriwijaya University, Jl. Srijaya Negara Palembang 30139, Indonesia

[2]Chemical Engineering Department, Sriwijaya University, Jl. Raya-Palembang-Prabumulih Ogan Ilir 30662, Indonesia

[3]Chemical Engineering Study Program, Palembang Muhammadiyah University, Jl. Jend. A. Yani 13 Ulu Palembang 30137, Indonesia

*subriyer@unsri.ac.id

Abstract. This study focuses on the removal of barium ions (Ba^{2+}) from produced water, a common challenge in industrial wastewater treatment due to barium's toxicity and scaling potential. To address this, the research introduces a novel ceramic composite adsorbent formulated from natural clay and residue catalytic cracking (RCC) spent catalyst, combining low cost, sustainability, and enhanced adsorption performance. The main objective is to evaluate the adsorption efficiency of this composite in a fixed-bed column system under varying operational conditions, while also modeling its dynamic behavior. Produced water with an initial barium concentration of 0.58 mg/L (pH 8.8) was fed in up-flow mode at flow rates of 6, 7, and 8 mL/min using a peristaltic pump. Effluent samples collected over 180 minutes were analyzed by UV- Vis. spectrophotometry. Results showed that lower flow rates increased contact time and improved adsorption efficiency, with breakthrough delayed to ~210 minutes at 6 mL/min compared to 160 minutes at 8 mL/min. Breakthrough modeling indicated that the Thomas model best represented the data ($R^2 \geq 0.95$), while the Yoon–Nelson model reliably predicted 50% breakthrough time. This work demonstrates that clay–RCC ceramic composites are effective, low-cost, and sustainable adsorbents.

Keywords: barium removal, fixed-bed adsorption, ceramic adsorbent, produced water, breakthrough curve

(Received 2025-07-19, Revised 2025-09-08, Accepted 2025-10-08, Available Online by 2025-10-31)

1. Introduction

Produced water is water co-extracted with oil and gas from porous geological formations and often occurs in large volumes, especially when enhanced oil recovery methods are applied [1–3]. This water, also known as formation water, is a complex mixture containing hydrocarbons, organic matter, salts, oil and grease, total dissolved solids, and various heavy metals [4]. On a global scale, the oil and gas industry generates around 250 million barrels of produced water per day, and over 40% of it is directly discharged into the environment, particularly from offshore operations [5]. Without adequate treatment, produced water poses a serious risk to surface water quality and aquatic ecosystems.

Among the heavy metals commonly found in produced water, barium frequently exceeds the safe limit of 2 mg/L [6]. Naturally present in geological formations as barite ($BaSO_4$), barium enters formation water during oil and gas drilling and production activities. Barium is highly reactive, forming insoluble sulfate scales that clog pipelines and equipment [7–9]. In addition, high barium concentrations may indicate the presence of naturally occurring radioactive materials (NORM) such as Radium-226 and Radium-228 [10]. In aquatic environments, barium can bioaccumulate and biomagnify, disrupting benthic ecosystems and threatening public health due to its links with kidney and cardiovascular disorders [11].

Several techniques have been employed for the removal of barium from wastewater, including chemical precipitation, ion exchange, membrane filtration, and adsorption. Chemical precipitation using sulfate or carbonate reagents is effective but generates large amounts of sludge, creating disposal challenges [6]. Membrane-based technologies such as nanofiltration and reverse osmosis provide high removal efficiency but are limited by high operating pressures, energy costs, and frequent maintenance requirements [6]. Ion exchange resins can also achieve significant barium removal; however, they are prone to fouling and require costly regeneration, making them less practical for large-scale applications [6]. In comparison, ceramic-based adsorbents present a cost-effective, environmentally friendly, and sustainable alternative. Clay- or waste-derived ceramics, such as RCC–clay composites, offer advantages including thermal stability, mechanical durability, and tunable surface properties that enhance adsorption capacity [6]. These attributes justify the application of ceramic adsorbents in fixed-bed column systems as a practical and economical solution for barium removal from produced water.

Several technologies have been developed to remove barium from water. Previous studies have explored various adsorbents for barium removal, including zeolites, activated carbon, and agricultural waste [12,13]. Chemical methods using chelating agents or potassium salts can enhance barite solubility [8,14,15], adsorption [16], and adsorption using metal organic framework [17], while membrane-based processes like reverse osmosis (RO) and nanofiltration offer high removal efficiency [4]. However, these technologies often face limitations such as high costs and membrane fouling. Recent advances in functional materials, such as MOFs and MXene-based adsorbents, show excellent barium removal performance but remain costly and complex to synthesize [17,18].

Natural clay is abundant and chemically suitable for adsorption, while the residue catalytic cracking (RCC) spent catalyst, a silica-and alumina-rich waste from oil refinery units, is promising as a ceramic adsorbent component. However, limited attention has been paid to waste-derived ceramic adsorbents. RCC, a waste product from petroleum refining, combined with naturally available clay, offers a promising material due to its porosity and surface reactivity. In South Sumatra alone, one refinery produces approximately 15.98 tons of RCC waste annually [19], yet much of it remains underutilized and classified as hazardous waste.

This study introduces a novel approach by utilizing spent residue catalytic cracking (RCC) catalyst, an abundant industrial waste, combined with natural clay to fabricate low-cost ceramic adsorbents for barium removal from produced water. The integration of ceramic adsorbents with reverse osmosis (RO) membranes in a hybrid system aims to enhance overall barium removal while mitigating membrane fouling.

This research contributes to the growing body of work on ceramic-based adsorbents by demonstrating the potential of integrating waste-derived materials into functional adsorption systems. While previous studies have primarily focused on conventional ceramics such as kaolin, fly ash, or zeolite-based

composites, the utilization of RCC spent catalyst in combination with natural clay provides a novel, sustainable alternative with both economic and environmental benefits. By repurposing a silica- and alumina-rich refinery waste into a porous, reactive ceramic adsorbent, this study not only addresses the challenge of hazardous waste management but also advances the development of cost-effective materials for heavy-metal remediation. Moreover, the hybridization of ceramic adsorbents with reverse osmosis membranes introduces an innovative strategy that enhances barium removal efficiency and mitigates fouling, thereby broadening the application scope of ceramic adsorbents in water treatment.

2. Methods

2.1 Materials

Produced water samples were collected from an oil and gas facility located in South Sumatra, Indonesia. The residue catalytic cracking (RCC) spent catalyst, with a particle size of 100 mesh, was supplied by a local crude oil processing company in the same region. Ceramic adsorbents were synthesized by combining RCC spent catalyst (50%) and natural clay (50%), followed by molding the mixture into cylindrical tablets with diameters of 1 cm and 2 cm, each with a thickness of 1 cm. To remove suspended solids, polypropylene (PP) sediment filters with pore sizes of 0.5, 0.3, and 0.1 μm were installed upstream of the adsorption column.

The ceramic adsorbents were introduced into a fixed-bed column with a diameter of 10 cm and a packing height of 30 cm, corresponding to a packing mass of approximately 2.1–2.3 kg, depending on particle size distribution. After adsorption treatment, the column effluent was subjected to reverse osmosis (RO) using a CSM RE 4040 BE membrane, which has dimensions of 10.16 cm in diameter and 101.6 cm in length. The membrane system operated at a flow rate of 9.3 m^3/day under a maximum pressure of 4.14 MPa, with chlorine levels kept below 0.05 mg/L to prevent chemical damage to the membrane. To examine surface structure and elemental composition, the adsorbents were analyzed by scanning electron microscopy coupled with energy-dispersive X-ray spectroscopy (SEM–EDX), employing a Hitachi Flex Sem 1000 and Thermo Scientific Axia system.

2.2 Methods

The produced water treatment process developed in this study was conducted in three sequential stages. The first stage involved preliminary filtration of produced water using a PP sediment filter to remove suspended solids from the samples. In the second stage, adsorption was carried out employing ceramic-based adsorbents synthesized from a combination of natural clay and RCC, prepared in various compositional ratios. The final stage of treatment utilized reverse osmosis (RO) membrane filtration to further reduce the barium concentration.

Table 1 provides a summary of the composition and diameter of each adsorbent variant used in the experiment.

Table 1. Composition ratios and physical dimensions of ceramic adsorbents

Adsorbent	Clay (%)	RCC (%)	Diameter (cm)
A	50	50	1
B	50	50	2

Barium content was examined using an atomic absorption spectrophotometer (AAS). The initial concentration of barium in the produced water sample is 0,58 mg/L. Barium removal efficiency was derived by employing the following formula:

$$\eta\,(\%) = \left(\frac{C_1 - C_2}{C_1}\right) x\ 100 \qquad (1)$$

Where: C_1 is the inlet concentration, and C_2 is the outlet concentration. The detailed design and layout of the experimental unit have been described previously [20], including images of the ceramic adsorbent configuration.

Adsorption experiments were conducted in both batch and continuous column modes to evaluate the barium removal performance of ceramic adsorbents. Batch tests were performed to determine adsorption capacity and equilibrium behavior under controlled mixing, while fixed-bed column experiments simulated dynamic flow conditions, assessing breakthrough behavior at flow rates of 6–8 mL/min. Each experiment was carried out in triplicate, and the results are reported as mean values with associated standard deviations. Model fitting for breakthrough curves was evaluated using regression analysis, with R^2 values > 0.95 indicating excellent agreement between experimental and theoretical predictions.

Regeneration studies were also performed to assess the reusability of the ceramic adsorbents. After saturation, the adsorbents were washed with 0.1 M HCl solution, followed by rinsing with deionized water until a neutral pH was achieved. The regenerated adsorbents were subsequently reused in column experiments for up to three cycles, showing only a minor reduction in adsorption efficiency (<10%).

3. Results and Discussion

3.1 Characterization of ceramic adsorbents

To assess the structural properties and composition of ceramic adsorbents, surface morphology and element distribution were characterized using SEM–EDX, as well as characterization of chemical functional groups using FTIR. This complementary characterization approach provides important insights into the adsorbent capacity and binding mechanism of barium ions from the resulting wastewater.

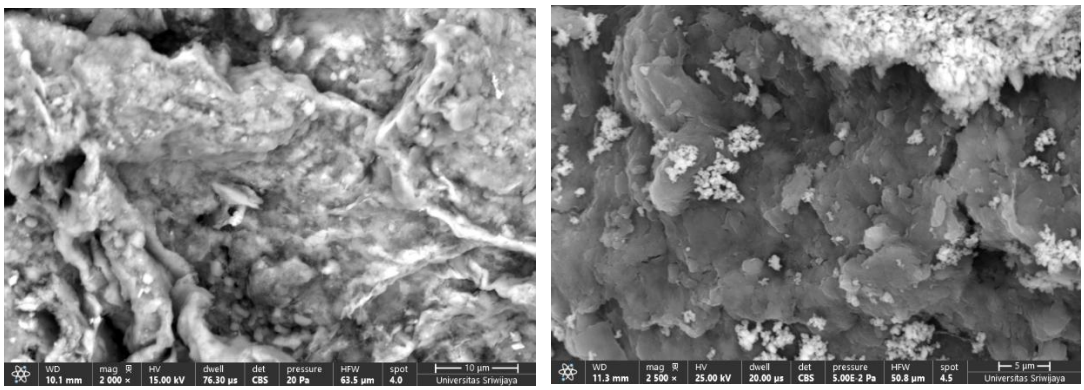

(a) (b)

Figure 1. SEM images of the adsorbent surface: (a) before barium adsorption and (b) following barium adsorption

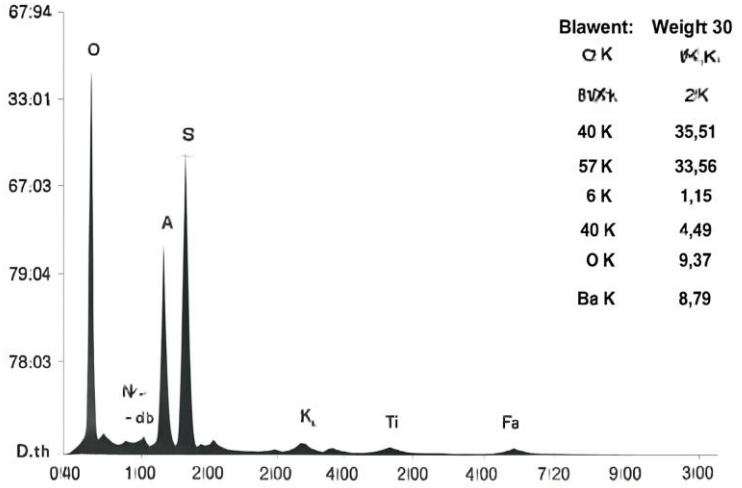

(a)

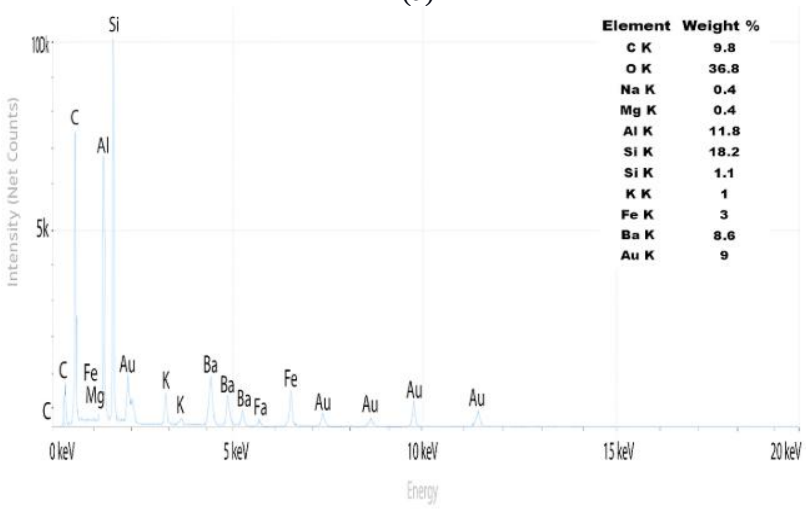

(b)

Figure 2. EDX image a) before Barium Adsorption and b) after Barium Adsorption

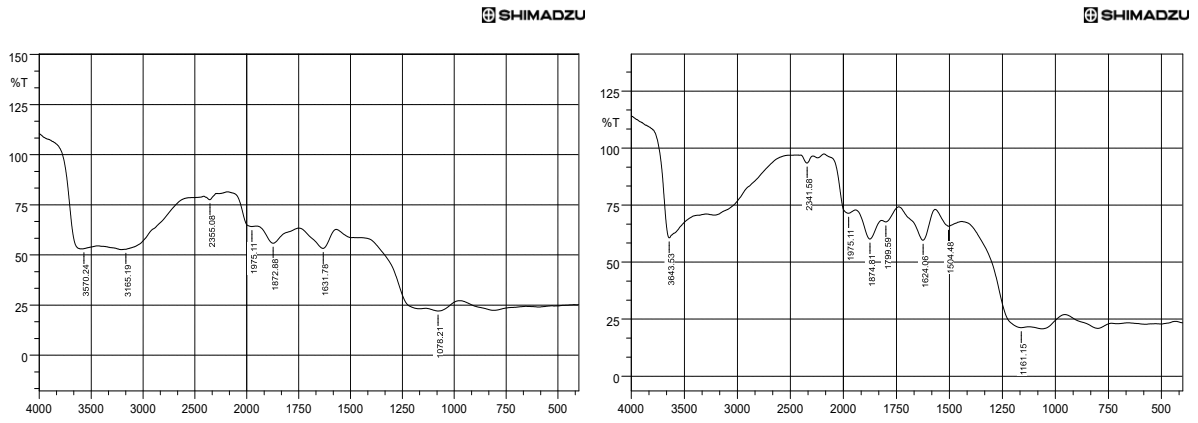

(a) (b)

Figure 3. FTIR image: a) before and b) after Barium adsorption

SEM images taken before adsorption (Figure 1) reveal a largely smooth and compact ceramic surface with very little porosity, suggesting that the adsorption active sites remain accessible. The uniform distribution of particles indicates the stability of the structure formed during calcination from a blend of RCC and natural clay in equal proportions. The corresponding EDX spectrum (Figure 3) verifies that the primary constituents of this material include oxygen (O), silicon (Si), and aluminum (Al), highlighting the aluminosilicate characteristics of both clay and FCC catalyst waste. Minor elements like sodium (Na), magnesium (Mg), potassium (K), and iron (Fe) were also identified, which are typically present in natural clay minerals and industrial byproducts.

Following the barium adsorption procedure, the surface of the adsorbent experiences considerable changes in its structure, as illustrated in Figure 1. The surface appears rougher and less uniform, featuring a buildup of granules and the blocking of pores, which demonstrates the effective adsorption of barium ions. The EDX spectrum recorded after the adsorption process (Figure 2) reinforces this observation with the appearance of new peaks within the energy range of 4.4–4. 8 keV, specifically indicating the presence of barium (Ba), which was not observed before adsorption. Furthermore, there is a noticeable adjustment in the intensity of the peaks for iron (Fe) and gold (Au), with gold likely originating from the conductive layer applied during SEM sample preparation. These alterations in both morphology and composition highlight the capability of capturing barium, aligning with the chemomorphic mechanism suggested by the pseudo-order two kinetics model.

Additional chemical analysis was carried out using FTIR spectroscopy to study how the surface functional groups interact with Ba^{2+} ions. FTIR spectroscopy was utilized to detect the functional groups on the surface of the ceramic adsorbent both before and following the process of barium adsorption. This examination offers insight into how the adsorbent surface interacts with the barium ion.

Before starting the adsorption process, the FTIR spectrum revealed several distinct absorption peaks. The broad absorption bands are located around 3620. 24 cm^{-1} and 3166. 61 cm^{-1} are indicative of stretching vibrations linked to the O–H group, which is typically associated with hydroxyl groups on the surface and adsorbed water molecules. These areas are recognized as active sites where metal ions may bind. The absorption peak at 2356. 98 cm^{-1} corresponds to the asymmetric stretching vibrations of CO_2, likely resulting from air pollution or the presence of carbonates. Moreover, the peaks at 1872. 88 cm^{-1} and 1631. 78 cm^{-1} represents the bending vibrations of H–O–H and variations in the Al–OH group, implying the presence of coordinated water or aluminum species. The prominent absorption peak at 1078. 21 cm^{-1} reflects the asymmetric stretching vibrations of Si–O–Si or Si–O–Al, confirming the existence of the silicate framework in both the clay materials and the waste produced by the RCC catalyst.

After the barium adsorption procedure, the FTIR spectrum revealed a notable change in both the strength and the position of the peaks, indicating a strong bond between barium ions and the functional

groups located on the surface of the ceramic material. The O–H bands around 3620 and 3166 cm^{-1} showed diminished intensity, suggesting that hydroxyl groups are involved in the binding of barium. The CO_2 band at 2356. 98 cm^{-1} was less pronounced, probably due to the development of barium complexes. The peaks within the 1872–1631 cm^{-1} range became wider and slightly shifted, which might indicate changes in the structure of the adsorbent surface following its interaction with Ba^{2+}. The most significant alteration was observed in 1078. 21 cm^{-1} band, where there was a considerable decrease in intensity, reinforcing the notion that Si–O and Al–O groups are engaged in either complexation or ion exchange with barium.

The overall changes in the spectra confirm that barium ions are effectively attached to the ceramic adsorbent surface via a chemical adsorption process. This interaction involves functional groups like surface hydroxyls, silanol, and aluminium hydroxyls, which create sites for barium ions by forming chemical complexes or through electrostatic forces. These results align with earlier-mentioned kinetic and isothermal models, specifically the pseudo-second order (PSO) model and Langmuir isotherms, which substantiate the presence of chemical monolayer adsorption on reactive surfaces.

3.2 Adsorption study on fixed-bed columns

The adsorption studies were conducted in a fixed-bed setup using vertically positioned glass columns measuring 10 cm in internal diameter and 40 cm in total height. The columns were uniformly packed to a depth of 30 cm with a 1:1 blend of natural clay and recycled ceramic waste as the adsorbent medium. Produced water containing barium at an initial concentration of 0.58 mg/L and a pH of 8.8 was pumped upward through the column using a peristaltic pump, with flow rates regulated at 6, 7, and 8 mL/min to ensure stable operation.

Effluent samples were withdrawn every 15 minutes for a period of 180 minutes, and barium levels were determined spectrophotometrically with an Agilent Cary 60 UV-Vis at a detection wavelength of 282 nm.

3.3 Adsorption Column Data Analysis

The data obtained from the fixed flow column experiment was applied to model the breakthrough curve by plotting the ratio of outlet to inlet concentration (Ct/Co) as a function of time. The breakthrough curve describes the adsorption process continuously and can be used to determine the breakthrough time (tb) when Ct/Co = 0.1 (10%) and the saturation time (te) when $\frac{C_t}{C_0}$ = 0.9 (90%).

The saturation time (te) and breakthrough time (tb) can be calculated using Equations (2) and (3), respectively.

The total amount of adsorbed Barium adsorbate in the column (mg) is determined from the area below the breakthrough curve, as described in Equation (3):

$$q_{total} = Q \times \int_0^{t_e} (C_o - C_t)\, dt \qquad (2)$$

Where:

q_{total}: total mass of adsorbed Barium (mg), Q: volumetric flow rate (mL/min), C_o and C_t: initial concentration and at time t (mg/L), t_e: Saturation time (minutes)

The breakthrough time (t_b) is defined as the time at which the outlet concentration (Ct) reaches a specific fraction of the inlet concentration (C_0), commonly when $\frac{C_t}{C_o}$ = 0.05 or 5%. A shorter breakthrough time indicates a faster saturation of the adsorbent bed, typically associated with higher flow rates or reduced contact time. Conversely, longer breakthrough times reflect more efficient adsorption due to extended residence time within the column. An increase in flow rate resulted in earlier breakthrough, demonstrated by a more rapid rise in the C_t/C_0 ratio. This behavior suggests that higher flow velocities limit the time available for diffusion and surface interaction, thereby decreasing overall adsorption efficiency.

A detailed summary of the experimental results, including breakthrough times and flow rate effects, is presented in Table 2.

Table 2. Effluent Concentration (Ct) and Ct/Co Ratio as a Function of Time at Different Flow Rates

	6 mL/min	7 mL/min	8 mL/min	6 mL/min	7 mL/min	8 mL/min
t	Ct			Ct / Co		
0	0	0	0	0	0	0
15	1.3296	1.2222	1.4427	0.0	0.0	0.0
30	1.7363	1.8269	1.9149	0.0	0.0	0.0
45	3.1067	4.2647	3.4041	0.1	0.1	0.1
60	7.1637	7.9148	8.8356	0.1	0.1	0.2
75	9.3247	10.8479	12.976	0.2	0.2	0.2
90	24.000	27.162	29.962	0.4	0.5	0.5
105	29.998	33.430	36.910	0.5	0.6	0.6
120	36.458	38.794	41.854	0.6	0.7	0.7
135	39.474	41.244	43.304	0.7	0.7	0.7
150	41.156	42.998	44.826	0.7	0.7	0.8
165	41.968	42.984	45.942	0.7	0.7	0.8
180	42.664	43.764	46.142	0.7	0.8	0.8

Figure 4 illustrates the dynamics of the barium ion adsorption process in a fixed flow column with variations in flow rate based on Table 2. The curve provides important information about the timing of the breakthrough and the adsorption efficiency in each operating condition.

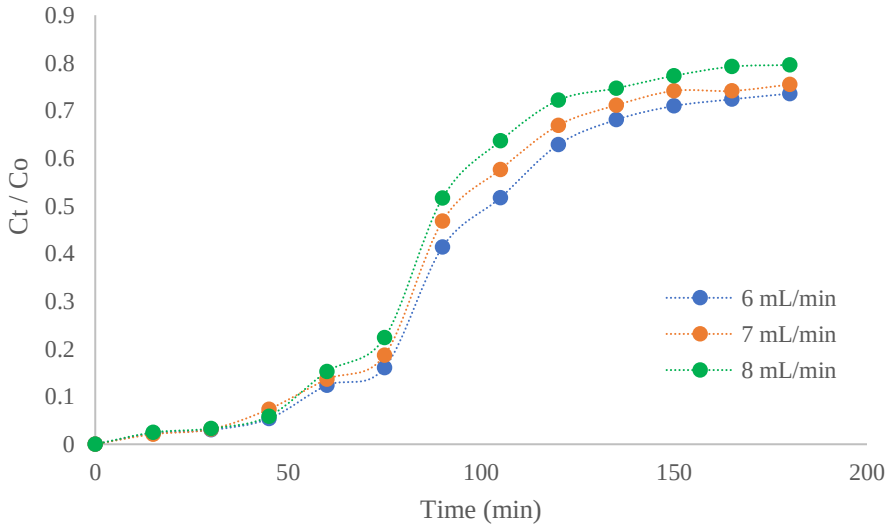

Figure 4. Breakthrough curve of barium removal

The breakthrough profile in Figure 4 highlights the significant influence of flow rate on the onset of breakthrough. At a lower flow rate of 6 mL/min, breakthrough was observed at roughly 30 minutes, whereas at increased flow rates of 7 and 8 mL/min, the breakthrough point shifted earlier, occurring at around 45 and 15 minutes, respectively. This behavior illustrates that higher flow rates shorten the interaction time between barium ions and the adsorbent, leading to faster column exhaustion. Additionally, the curve shape reflects adsorption dynamics through the mass transfer zone (MTZ): slower flow rates promote a broader MTZ due to enhanced diffusion and contact, while faster flow conditions compress the MTZ, accelerating saturation [21]. Model fitting analysis revealed that the

Thomas model provided the best agreement with experimental data ($R^2 \geq 0.95$), suggesting that adsorption is governed by both mass transfer and surface equilibrium mechanisms. Meanwhile, the Yoon–Nelson model reliably predicted the 50% breakthrough time (τ), in line with recent findings for heavy metal removal in fixed-bed systems [21]. These results highlight the importance of flow rate optimization and model-based interpretation for scaling up adsorption processes in industrial wastewater treatment.

This event corresponds to the idea of adsorption kinetics in systems with continuous flow, where increased flow speeds and shorter residence times reduce the chances of metal ions bonding with the active sites of the adsorbent [21]. Consequently, the performance of adsorption tends to improve with slower flow rates, as shown by the graph depicting a longer breakthrough time at 6 mL/min.

These results are consistent with previous studies, which have demonstrated that lower flow rates provide a longer contact time between the adsorbate and the adsorbent's surface, thereby increasing adsorption capacity and delaying the column's saturation [22]. The prolonged residence time at slower flow rates enhances diffusion and interaction with the surface, leading to a more efficient utilization of the active sites within the adsorbent material.

3.5 Kinetic models on fixed column systems

Adsorption kinetics of fixed column systems has an important role in evaluating and describing the performance of the adsorption process. These models are not only used to predict the dynamics of mass displacement, but also to assess the effectiveness of the type of adsorbent as well as the column design used, so that they can be used in large-scale process optimization [24–26].

In this study, the three kinetic models used to analyze the experimental data are the Thomas model, the Adam-Bohart model, and Yoon–Nelson model. Both models were chosen because they have been widely used in dynamic adsorption studies and provide a mathematical approach that is appropriate for fixed-flow column systems.

The linear shape of each model is presented in the Equation

3.5.1 Thomas Model

Model Equation:

$$\ln\left[\left(\frac{C_0}{C_t}\right) - 1\right] = k_{Th}x\, q_0 x \left(\frac{m}{Q}\right) - k_{Th}x\, C_0 xt \qquad (3)$$

Where: C_0= inlet concentration (mg/L), Ct= effluent concentration at time t (mg/L), k_{Th}= Thomas rate constant (mL/min·mg), q_0= maximum adsorption capacity (mg/g), m= mass of adsorbent (g), Q= flow rate (mL/min), and t = time (min)

The Thomas model assumes Langmuir-type kinetics with plug flow conditions and negligible axial dispersion. A plot of $\ln\left[\left(\frac{C_0}{C_t}\right) - 1\right]$ Versus time yields a straight line if the Model fits the data well, allowing for the estimation of k_{Th} and q_0. In this study, the high R^2 values (>0.95) indicate excellent Model fit, suggesting that the adsorption process follows second-order reversible kinetics. This Model is handy for predicting column performance and optimizing operational parameters.

3.5.2 Adams-Bohart Model

Model Equation:

$$\ln\left(\frac{C_0}{C_t}\right) = k_{AB}x\, C_0 xt - K_{AB}x\, N_0 x\frac{z}{U} \qquad (4)$$

Where: k_{AB}= Adams-Bohart rate constant (L/mg.min), N_0= maximum volumetric sorption capacity (mg/L), z = bed depth (cm), U= linear velocity (cm/min), t= time (min)

The Adams–Bohart model is best suited for describing the onset of adsorption in fixed-bed systems. It captures the initial segment of the breakthrough curve by assuming that the adsorption rate is proportional to both the unoccupied adsorption sites and the influent solute concentration. From the linearized form of the model, the key parameters—the rate constant (k_AB) and the maximum sorption capacity per unit volume (N_0)—can be derived from the slope and intercept. Its effectiveness in

illustrating the early breakthrough stage highlights the critical roles of bed depth and flow velocity in determining the overall efficiency of the adsorption column.

3.5.3 Yoon-Nelson Model

Model Equation:

$$\ln\left[\frac{C_t}{(C_o - C_t)}\right] = K_{YN}(t - \tau) \quad (5)$$

Where: C_o, C_t= initial and effluent concentrations (mg/L), K_{YN}= rate constant (1/min), τ= time required for 50% breakthrough (min), t = time (min)

The Yoon-Nelson model provides a simplified approach that does not require detailed column characteristics. It assumes that the probability of adsorbate breakthrough is proportional to the remaining adsorption capacity. The linear plot of $\ln\left[\frac{C_t}{(C_o - C_t)}\right]$ versus t allows for direct calculation of K_{YN} and τ. A high R^2 value confirms the Model's validity and supports the assumption that the adsorption mechanism is predominantly governed by first-order kinetics.

3.6 Model Adams–Bohart

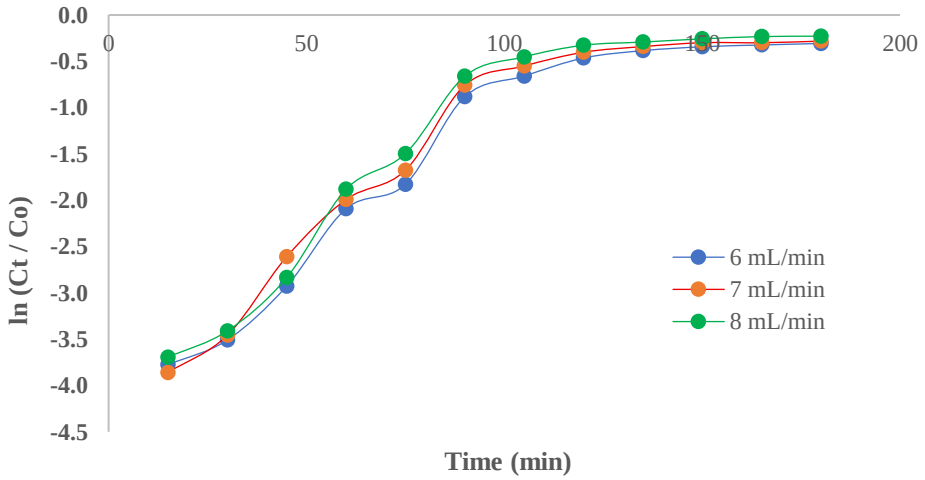

Figure 5. Adam-Bohart Kinetic Model

The Adams–Bohart model is commonly applied to represent the initial stage of fixed-bed adsorption, based on the assumption that the adsorption rate depends on both the available capacity of the adsorbent and the concentration of the incoming solute. In this work, the model provided a reasonable fit at a flow rate of 6 mL/min (R^2 = 0.883), but its accuracy diminished as the flow rate increased. This outcome aligns with previous reports noting that the Adams–Bohart model is best suited for describing the early breakthrough period and is less reliable for the complete adsorption profile, largely because it does not incorporate the effects of equilibrium saturation [22]. A comparative performance summary of adsorption models is presented in Table 1, highlighting the model fit in this study relative to literature benchmarks. The Thomas model consistently showed the best correlation ($R^2 \geq 0.95$), followed by the Yoon–Nelson model, which provided reliable estimation of 50% breakthrough time. The Adams–Bohart model, however, is less robust for long-term predictions, confirming its utility only for the early breakthrough region.

Table 3. Comparative Performance

Model	R^2 (This Study)	Key Prediction Strength	Limitation	Literature Support
Thomas	≥ 0.95	Overall breakthrough fit	Assumes Langmuir kinetics	Singh et al., 2021
Yoon–Nelson	≥ 0.93	50% breakthrough time	Less accurate for the full curve	Zhang et al., 2022
Adams–Bohart	0.88 (6 mL/min)	Early-stage adsorption	Weak for the equilibrium zone	Mohan et al., 2020

Several operational factors strongly influence model accuracy and column performance. Flow rate plays a critical role, as higher rates reduce residence time and limit the diffusion of Ba^{2+} ions into pore sites, resulting in faster breakthrough. Particle size is another determinant, as smaller particles provide a larger surface area and shorter intraparticle diffusion paths, improving adsorption kinetics but potentially increasing pressure drop across the column [22]. In addition, bed height and initial solute concentration affect the saturation dynamics, where taller beds and lower initial concentrations generally prolong breakthrough times [22].

Despite its utility, the Adams–Bohart model has notable limitations. It assumes negligible axial dispersion and homogeneous adsorbent characteristics, which may not hold in real produced-water systems containing complex matrices and competing ions. Moreover, fouling or clogging of the packed bed over extended operation can reduce porosity and limit long-term efficiency. Similarly, scaling up from laboratory-scale columns to industrial systems introduces challenges such as non-ideal flow patterns and adsorbent attrition, which are not accounted for in the model [22].

In summary, while the Adams–Bohart framework provides useful insights into the early dynamics of barium adsorption, its predictive scope is limited compared to the Thomas and Yoon–Nelson models. Future work should incorporate hybrid or modified models that can capture both the initial and equilibrium phases of adsorption under realistic operating conditions.

3.7 Thomas Model

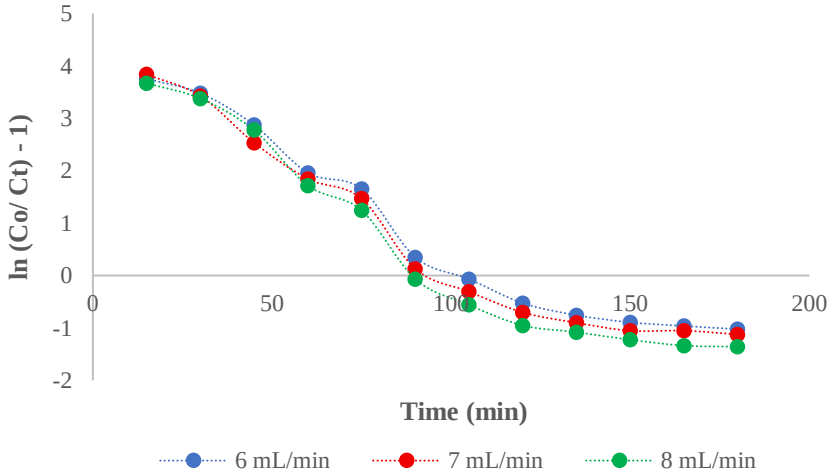

Figure 6. Thomas Kinetic model

The Thomas model is a widely utilized approach in designing adsorption columns due to its reliance on pseudo-order kinetics and plug flow assumptions. The model maintains a high level of accuracy at all flow rates, with R^2 consistently greater than 0.96, signifying a reliable and precise correlation with

the experimental data. Therefore, the Thomas model proves to be highly effective in column applications for estimating adsorption performance across diverse operational scenarios.

3.8 Model Yoon–Nelson

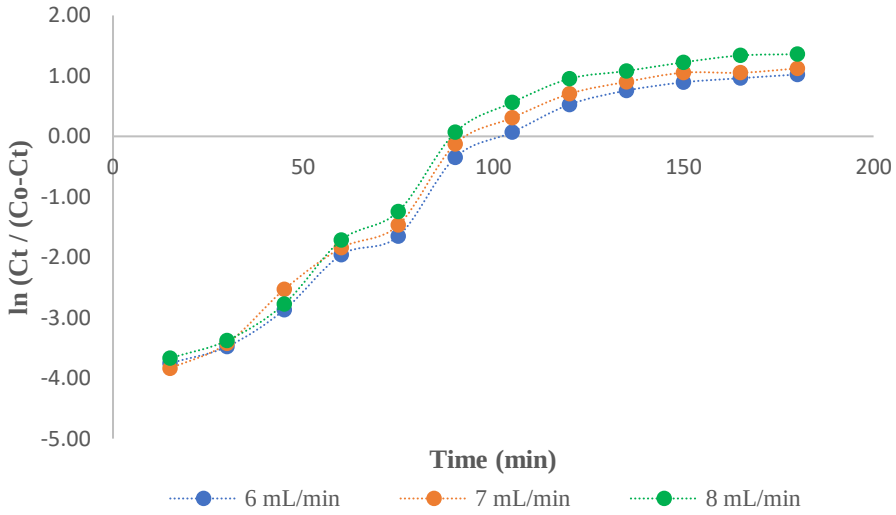

Figure 7. Yoon-Nelson Kinetics model

The Yoon–Nelson model provides a straightforward evaluation method since it requires only two parameters, the rate constant and the 50% breakthrough time (τ). Its predictive accuracy, reflected in R^2 values comparable to the Thomas model, indicates strong capability in characterizing breakthrough behavior. The stability of its parameters across different flow rates further highlights its reliability as a practical tool for column performance assessment. When comparing models, both Thomas and Yoon–Nelson produced excellent agreement with the experimental results, though the Thomas model showed a slight edge in precision due to its inclusion of adsorption capacity, which makes it highly relevant for process design at an industrial scale. Meanwhile, the Yoon–Nelson model, despite its simpler structure, still offered robust predictions and can be adopted as an efficient alternative for performance evaluation. On the other hand, the Adams–Bohart model was useful in describing the initial adsorption region but proved less effective in representing the full breakthrough curve. A comparative overview of these modeling outcomes is summarized in Table 3.

Table 3. Comparison of the results of the Thomas, Yoon-Nelson, and Adams-Bohart models

Flow Rate (mL/min)	Adams–Bohart–			Thomas			Yoon–Nelson		
	Slope (k_AB)	Intercept	R^2	Slope (k_Th)	Intercept	R^2	(k_YN)	Intercept	R^2
6	0.025	-3.251	0.883	-0.05	4.0	0.98	0.05	-4.0	0.98
7	0.021	-2.722	0.85	-0.05	3.5	0.97	0.05	-3.5	0.97
8	0.021	-2.571	0.786	-0.06	3.6	0.96	0.06	-3.6	0.96

The Adams–Bohart model is particularly good at explaining the initial stages of adsorption, but it loses precision as the flow rate rises. The R^2 value fell from 0.883 at 6 mL/min to 0.786 at 8 mL/min, indicating a diminishing ability of the model to accurately represent the entire breakthrough curve, particularly when contact times were shorter due to higher flow rates. In contrast, the Thomas model demonstrates strong consistency and correlation, with R^2 values exceeding 0.96 across all flow rates. The Thomas rate constant (k_Th) remains relatively constant, ranging from -0.05 to -0.06, indicating that the adsorption kinetics are not greatly affected by changes in flow rates within the tested range.

Similarly, the Yoon–Nelson model performs on par with the Thomas model, exhibiting the same R^2 values and stable parameters. The simplicity of this model is its key strength, as it relies on just one parameter (τ) to estimate the time required for a 50% breakout.

Overall, the Adams–Bohart model is helpful for early predictions, but less accurate at high flow rates. Meanwhile, the Thomas and Yoon–Nelson model is well-suited for comprehensive and applicable column performance modelling in real water treatment systems. As reported by [26,27], these models were also utilised in studies of blue methylene adsorption at Clay@Fe_3O_4, suggesting that the Thomas and Yoon–Nelson model provided the best fit, with R^2 values exceeding 0.96 under various operating conditions, which corroborates similar findings in this study. Similarly, [28] in their mathematical study of barium adsorption emphasised that the accuracy of the kinetic model is greatly influenced by operating conditions, which impact adsorbent saturation and breakthrough time.

Operational factors such as the duration of contact and the speed of flow significantly influence the adsorption process. The duration of contact allows for enough interaction between the adsorbate and the adsorbent, whereas the flow rate impacts both the length of exposure and the speed of mass transfer. It is essential to optimize these elements to enhance removal efficiency. In this section, we examine how changes in contact time and flow rate influence the efficiency of barium removal using ceramic-based adsorbents made from clay and RCC spent catalyst, as well as their combination with reverse osmosis (RO). The evaluation employs batch adsorption experiments and column breakthrough tests for ongoing adsorption to shed light on the dynamic behavior of barium uptake across various operational conditions.

3.9 Effect of contact time and flow rate on barium removal in standalone and hybrid systems

The integration of the column adsorption process with reverse osmosis (RO) showed a significant increase in barium allowance. After the RO filtration stage, the concentration of barium in the output water dropped to 0.104 mg/L, well below the WHO threshold of 2 mg/L. The total efficiency of the hybrid system reached 99.82% at a flow rate of 6 L/min and a contact time of 60 minutes.

The advantage of this system lies in the synergy between the adsorption and RO processes. Early adsorption lowers the contaminant load, reducing the potential for fouling on the RO membrane. In contrast, RO enhances the separation of ions that escape from the adsorbent. This integration is proven to improve technical performance and extend the life of the membrane.

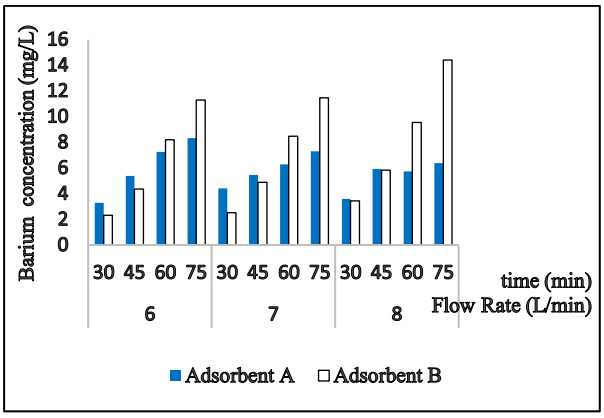

(a)

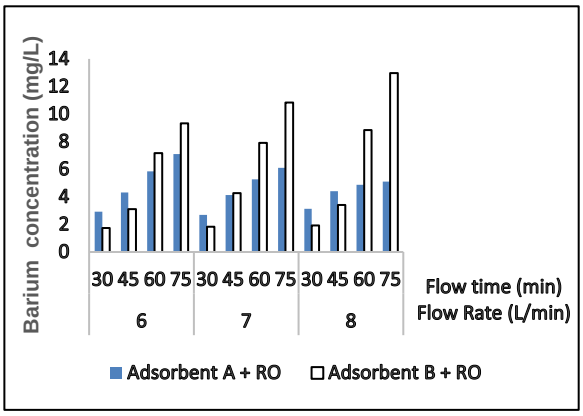

(b)

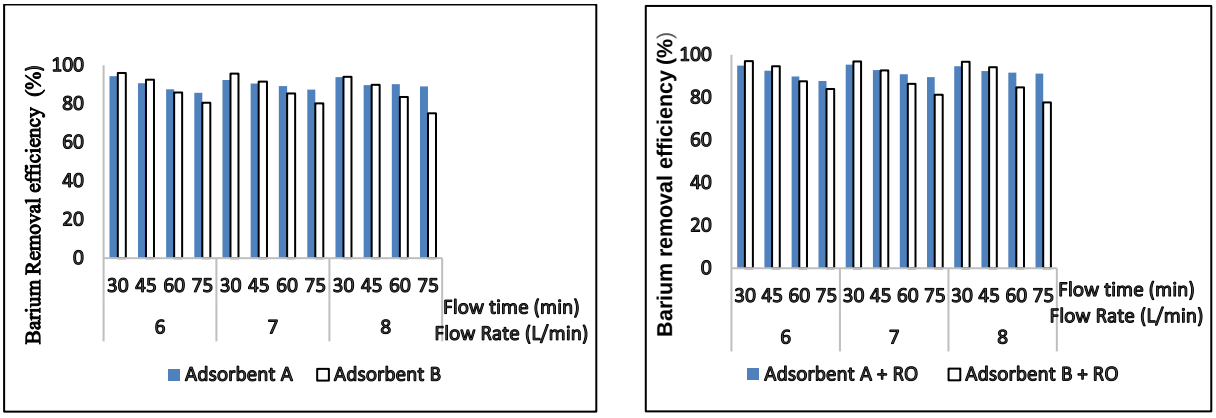

(c) (d)

Figure 8. Effect of contact time and flow rate on barium concentration (Figures 8a and 8c) and removal efficiency (Figures 8b and 8d) using ceramic adsorbents, both as a standalone treatment and in combination with RO.

In Figure 8a, a notable decline in barium concentration was observed during the initial 30 minutes of contact, particularly at a flow rate of 6 mL/min. Adsorbent A reduced the barium concentration to 3.30 mg/L (94.31%), while adsorbent B performed even better at 2.32 mg/L (96%). These results indicate the rapid uptake of Ba^{2+} ions within the early phase of interaction, attributed to the high availability of active sites. However, extending contact time beyond 30 minutes showed only marginal improvements, suggesting the onset of surface saturation or even partial desorption, especially evident in adsorbent B. At higher flow rates (7 and 8 mL/min), the adsorption efficiency declined across all contact durations. For example, at 8 mL/min and 75 minutes, the remaining barium concentration for adsorbent A increased to 6.38 mg/L (89%), whereas adsorbent B's performance dropped sharply to 14.4 mg/L (75.17%). This trend is attributed to a shortened hydraulic residence time and intensified flow turbulence, which disrupts the mass transfer boundary layer and hinders ion diffusion onto the adsorbent surface, corroborating findings by [29], [3].

Figure 8b highlights that most ceramic adsorbents maintained barium removal efficiencies above 80%**,** with optimal performance at 60 minutes and 6 mL/min flow rate. Prolonged contact time favors extended ion–adsorbent interactions, while higher flow rates lead to early breakthrough and lower adsorption due to channeling effects. Additionally, adsorbent geometry played a critical role: smaller-diameter cylindrical adsorbents consistently outperformed larger ones (2 cm). This observation is aligned with previous studies by [30], which showed improved metal uptake with reduced particle or adsorbent size.

In Figures 8c and 8d, the integration of ceramic adsorbents with RO membranes significantly enhanced barium removal efficiency, consistently achieving values above 90% across all conditions. At 6 mL/min, hybrid systems using adsorbent A and B achieved removal efficiencies of 94.97% (2.92 mg/L) and 97% (1.74 mg/L), respectively. Interestingly, at higher flow rates, RO still maintained high removal performance, especially for adsorbent B at 8 mL/min, reaching 77.62% removal. This indicates the robustness of the hybrid system even under more challenging hydraulic conditions.

Overall, the integration of ceramic adsorption with RO not only mitigates the limitations of standalone adsorption (such as saturation and desorption) but also ensures high-quality effluent that meets stringent regulatory standards. These findings emphasize the importance of optimizing flow rate and contact time to achieve maximum treatment efficiency in hybrid water purification systems.

4. Conclusion

The findings demonstrate that a hybrid adsorbent prepared from natural clay and spent residue catalytic cracking (RCC) catalyst can successfully capture barium ions from water when applied in a fixed-bed

column setup. Experiments conducted with a 10 cm column diameter, a 30 cm packing height, and flow rates of 6–8 mL/min showed that slower flow conditions promoted higher adsorption efficiency by allowing longer interaction between the solution and the adsorbent surface. Breakthrough curve analysis further indicated that lower flow rates postponed the breakthrough point, thereby extending the effective adsorption period. To analyze the dynamic behavior, three kinetic models—Thomas, Yoon–Nelson, and Adams–Bohart—were applied. The Thomas model exhibited the strongest agreement with experimental outcomes, supported by high determination coefficients ($R^2 \geq 0.95$). The Yoon–Nelson model also provided reliable predictions of the half-time breakthrough, whereas the Adams–Bohart model adequately captured the early adsorption process but became less precise as saturation progressed due to its simplified representation of mass transfer mechanisms.

In conclusion, the clay–RCC composite represents a cost-effective, sustainable, and efficient adsorbent for barium removal from industrial wastewater. To strengthen the practical applicability of this approach, future work should consider pilot-scale column experiments under real field conditions, enabling validation of adsorption efficiency, hydraulic performance, and regeneration under continuous operation. Further process optimization, including variations in bed height, particle size, and inlet concentration, would provide more accurate design parameters for scale-up. Additionally, the modification of the clay–RCC composite with functional groups, surface activation, or incorporation of other low-cost additives could be explored to enhance adsorption capacity and selectivity toward barium and other co-existing metal ions. These efforts will help establish the clay–RCC composite as a reliable material for sustainable wastewater treatment at an industrial scale.

References

[1] M. A. Al-Ghouti, M. A. Al-Kaabi, M. Y. Ashfaq, and D. A. Da'na, "Produced water characteristics, treatment and reuse: A review," *J. Water Process Eng.*, vol. 28, no. January, pp. 222–239, 2019, doi: http://10.1016/j.jwpe.2019.02.001.

[2] Igunnu & Chen, "Produced Water Treatment Technologies," *Int. J. Low-Carbon Technol.*, vol. 9, no. 3, pp. 157–177, 2012, doi: https://doi.org/10.1093/ijlct/cts049.

[3] Rusdi et al., "Total Dissolved Solids, Phenol, and Barium Removals from Oilfield Produced Water Using Kapok Fibers and Ultrafiltration Membrane," *Period. Polytech. Chem. Eng.*, vol. 67, no. 3, pp. 452–459, 2023, doi: https://doi.org/10.3311/PPch.21802.

[4] Ibrahim et al., "Advances in Produced Water Treatment Technologies: An In-Depth Exploration with an Emphasis on Membrane-Based Systems and Future Perspectives," *Water*, vol. 15, no. 16, p. 2980, 2023, doi: https://doi.org/10.3390/w15162980.

[5] Mahmoud & Salaheldin Elkatatny, "Removal of Barite-Scale and Barite-Weighted Water- or Oil-Based-Drilling-Fluid Residue in a Single Stage," *SPE Drill Compl*, vol. 34, no. 01, pp. 16–26., 2019, doi: https://doi.org/10.2118/187122-PA.

[6] A. A. Novira, S. Nasir, and F. Hadiah, "Produced Water Treatment Using The Residue Catalytic Cracking (RCC) Spent Catalyst As Ceramic Filter Material Integrated With Reverse Osmosis (RO) System," *J. Appl. Sci. Eng.*, vol. 26, no. 3, pp. 403–411, 2022, doi: http://10.6180/jase.202303_26(3).0011.

[7] Hussein et al., "Examining the factors that impact the formation of barite scale in water injection operations: experimental study and quantification of scale formation," *Discov. Appl. Sci.*, vol. 6, no. 10, 2024, doi: https://doi.org/10.1007/s42452-024-06176-7

[8] J. Al Jaberi *et al.*, "Minimizing the Barite Scale in Carbonate Formations during the Filter Cake Removal Process," *ACS Omega*, 2022, doi: 10.1021/acsomega.2c01339

[9] Dai et al, "Prediction Models of Barite Crystallization and Inhibition Kinetics: Applications for Oil and Gas Industry," *Sustain.*, vol. 13, no. 15, p. 8533, 2021, doi: https://doi.org/10.3390/su13158533.

[10] Ahmad et al., "Fate of radium on the discharge of oil and gas produced water to the marine environment," *Chemosphere*, vol. 273, p. 129550, 2021, doi: https://doi.org/10.1016/j.chemosphere.2021.129550.
[11] J. Kravchenko, T. H. Darrah, R. K. Miller, H. K. Lyerly, and A. Vengosh, "A review of the health impacts of barium from natural and anthropogenic exposure," *Environ. Geochem. Health*, 2014, doi: 10.1007/s10653-014-9622-7.
[12] Zsirka, B., et al. "Heavy metal adsorption by mechanically activated red mud: batch study," *J. Environ. Chem. Eng.*, vol. 9, no. 6, p. 106450, 2021, doi: https://doi.org/10.1016/j.jece.2021.106450.
[13] Barbosa et al., "Phytoremediation in flooded environments: Dynamics of barium absorption and translocation by Eleocharis acutangula," *Chemosphere*, vol. 219, pp. 836–844, 2019, doi: https://doi.org/10.1016/j.chemosphere.2018.12.07.4
[14] Bageri et al, "Toward a Complete Removal of Barite (Barium Sulfate BaSO4) Scale Using Chelating Agents and Catalysts," *Arab. J. Sci. Eng.*, vol. 42, pp. 1667–1674, 2017, [Online]. Available: https://link.springer.com/article/10.1007/s13369-017-2417-2.
[15] Z. Luo *et al.*, "A chelating agent system for the removal of barium sulfate scale," *J. Pet. Explor. Prod. Technol.*, 2020, doi: 10.1007/s13202-020-00886-5.
[16] M. I. Aly, M. R. Hassan, M. M. Ghobashy, and B. A. Masry, "Removal of barium (II), cobalt (II), and strontium (II) from aqueous solution using chemically modified poly (acrylonitrile-butadiene-styrene) pellets," *Part. Sci. Technol.*, 2022, doi: 10.1080/02726351.2021.1992060
[17] J. Hou, F. AlGhunaimi, T. P. Huang, and N. Aljuryyed, "An Effective Metal Organic Framework (MOF) for Selective Barium Removal from Oil Field Waters," 2024. doi: 10.2523/IPTC-24302-MS.
[18] Kang et al., "Sulfate-Rich Metal–Organic Framework for High Efficiency and Selective Removal of Barium from Nuclear Wastewater," *ACS Publ.*, vol. 56, no. 46, pp. 13866–13873, 2017, doi: https://doi.org/10.1021/acs.iecr.7b02887.
[19] R. E. D. Putri, S. Nasir, and F. Hadiah, "Application of Ceramic Filter and Reverse Osmosis Membrane for Produced Water Treatment," *Pollution*, vol. 8, no. 4, pp. 1103–1115, 2022, doi: http://10.22059/POLL.2022.337380.1343.
[20] N. Herawati, M. Hatta Dahlan, M. Yusuf, M. M. Iqbal, K. Ahmad Roni, and S. Nasir, "Removal of total dissolved solids from oil-field-produced water using ceramic adsorbents integrated with reverse osmosis," *Mater. Today Proc.*, vol. 87, no. 8, pp. 360–365, 2023, doi: http://10.1016/j.matpr.2023.03.624.
[21] Wang Jianlong and G. Xuan, "Adsorption kinetic models: Physical meanings, applications, and solving methods," *J. Hazard. Mater.*, vol. 390, p. 122156, 2020, doi: https://doi.org/10.1016/j.jhazmat.2020.122156.
[22] T. M. Budnyak, A. Slabon, and M. H. Sipponen, "Lignin–Inorganic Interfaces: Chemistry and Applications from Adsorbents to Catalysts and Energy Storage Materials," *ChemSusChem*, vol. 13, no. 17, pp. 4344–4355, 2020, doi: http://10.1002/cssc.202000216.
[23] Fernandez et al, "Experimental Design and Breakthrough Curve Modeling of Fixed-Bed Columns Utilizing a Novel 3D Coconut-Based Polyurethane-Activated Carbon Composite Adsorbent for Lead Sequestration," *Sustainability*, vol. 15, no. 19, p. 14344, 2023, doi: https://doi.org/10.3390/su151914344.
[24] Kannan,P et al. "Design of adsorption column for reclamation of methyldiethanolamine using homogeneous surface diffusion model," *Oil Gas Sci. Technol*, vol. 75, no. 82, p. 12, 2020, doi: https://doi.org/10.2516/ogst/2020073.
[25] M. S. Shafeeyan, W. M. A. W. Daud, and A. Shamiri, "A review of mathematical modeling of fixed-bed columns for carbon dioxide adsorption," *Chem. Eng. Res. Des.*, vol. 95, no. 5, pp. 961–988, 2014, doi: https://doi.org/10.1016/j.cherd.2013.08.018.
[26] Aboussabek et al., "Experimental investigation, kinetics and statistical modeling of methylene blue removal onto Clay@Fe3O4: Batch, fixed bed column adsorption and photo-Fenton degradation

studies," *Case Stud. Chem. Environ. Eng.*, vol. 9, p. 100580, 2024, doi: https://doi.org/10.1016/j.cscee.2023.100580.
[27] Odunola, B et al, "Adams-Bohart, Yoon-Nelson, and Thomas modeling of the fixed-bed continuous column adsorption of amoxicillin onto silver nanoparticle-maize leaf composite," *Appl. Water Sci.*, vol. 12 No 94, 2022, doi: https://doi.org/10.1007/s13201-022-01624-4.
[28] Carmel Jeeva Mary et al. "Study of Barium Adsorption from Aqueous Solutions Using Copper Ferrite and Copper Ferrite/rGO Magnetic Adsorbents," *Adsorpt. Sci. Technol.*, vol. 2022, p. 3954536, 2022, doi: https://doi.org/10.1155/2022/3954536.
[29] Rafiee, H., Sorbie, K. S., & Mackay, "The deposition kinetics of barium sulfate scale: Model development," *Front. Mater.*, vol. 10, p. 1198176, 2023, doi: https://doi.org/10.3389/fmats.2023.1198176.
[30] Cui, W. L *et al.*, "Regulating the particle sizes of NaA molecular sieves toward enhanced heavy metal ion adsorption," *New J. Chem.*, vol. 48, no. 17, pp. 7863–7874, 2024, doi: 10.1039/d3nj05924.
[31] Safian, P. Hashemi, and R. Heydari, "Adsorption of heavy metals from aqueous solutions by magnetic barium hydroxyapatite nanoparticles," *Int. J. Environ. Anal. Chem.*, vol. 105, no. 9, pp. 2146–2159, 2024, doi: 10.1080/03067319.2024.2306488.
[32] K. Castro and R. Abejón, "Removal of heavy metals from wastewaters and other aqueous streams by pressure-driven membrane technologies: An outlook on reverse osmosis, nanofiltration, ultrafiltration and microfiltration potential from a bibliometric analysis," *Membranes*, vol. 14, no. 8, p. 180, 2024, doi: 10.3390/membranes14080180.
[33] Q. Ma, J. Mu, X. Lv, J. Meng, H. Cui, Y. Qiu, H. Ruan, and J. Shen, "Sustainable recovery of ionic resources from resin regeneration wastewater: Long-term evaluation, membrane fouling analysis, and cleaning," *ACS ES&T Water*, vol. 3, no. 7, pp. 1855–1864, Sep. 2022, doi: 10.1021/acsestwater.2c00367.
[34] A. Mandal and S. P. S. Rajput, "Advances in alkali-activation of ceramic waste-based pozzolana in concrete and mortar: A comprehensive review," *Waste Biomass Valor*, vol. 16, pp. 3309–3330, 2025, doi: 10.1007/s12649-025-02993-y.
[35] S. O. Gutierrez-Reyna, E. C. Herrera-Hernández, C. G. Aguilar-Madera, M. V. López-Ramón, R. Ocampo-Perez, A. Parra-Marfil, E. Garcia-Hernandez, and E. Bailon-Garcia, "New trends in modelling of breakthrough curves to remove pollutants using adsorption on advanced monolith geometries," *Environmental Research*, vol. 243, p. 117871, Feb. 2024, doi: 10.1016/j.envres.2023.117871.
[36] K. H. Chu and M. A. Hashim, "Comparing different versions of the Yoon–Nelson model in describing organic micropollutant adsorption within fixed bed adsorbers," *Environmental Science and Pollution Research*, vol. 31, pp. 21136–21143, 2024, doi: 10.1007/s11356-024-32450-7.
[37] M. De Rosa, G. Filippone, T. M. Best, A. R. Jackson, and F. Travascio, "Mechanical properties of meniscal circumferential fibers using an inverse finite element analysis approach," *Journal of the Mechanical Behavior of Biomedical Materials*, vol. 126, p. 105073, Feb. 2022, doi: 10.1016/j.jmbbm.2022.105073.
[38] M. Danish, K. B. Ansari, R. A. Aftab, et al., "gPROMS-driven modeling and simulation of fixed bed adsorption of heavy metals on a biosorbent: benchmarking and case study," *Environmental Science and Pollution Research*, vol. 30, pp. 71511–71526, 2023, doi: 10.1007/s11356-021-13207-y.
[39] S. R. McIntyre, E. Hunter-Sellars, P. A. Saenz-Cavazos, A. R. Houghton, and D. R. Williams, "Novel zero-length column analysis of desorption curves for single cylindrical pellets," *Powder Technology*, vol. 416, p. 118207, Feb. 2023, doi: 10.1016/j.powtec.2022.118207.
[40] H. P. S. Costa, M. G. Oliveira, E. D. V. Duarte, et al., "Multi-walled carbon nanotubes green-functionalized with iron nanoparticles for continuous removal of pharmaceutical pollutants through fixed-bed adsorption: Integrated experimental and machine learning approaches," *Environmental*

Science and Pollution Research, vol. 32, pp. 18058–18075, 2025, doi: 10.1007/s11356-025-36716-6.

[41] G. O. Ogbeh, A. O. Ogunlela, C. O. Akinbile, and R. T. Iwar, "Adsorption of organic micropollutants in water: A review of advances in modelling, mechanisms, adsorbents, and their characteristics," Environmental Engineering Research, vol. 30, no. 2, p. 230733, Apr. 2025, doi: 10.4491/eer.2023.733.